FULL LENGTH PAPER

NUMERICAL SIMULATION OF FLOW FIELD OVER A SHARP-TIPPED DOUBLE CONE AT HIGH SPEED

R.C. Mehta
Department of Aeronautical Engineering
Noorul Islam University
Kumaracoil-629 180, India
Email : drrakhab.mehta@gmail.com

Abstract

The flowfield over a sharp-tipped double cone axisymmetric configuration is carried out by solving time dependent axisymmetric laminar compressible Navier-Stokes equations for freestream Mach number range of 2.0 - 6.0. The fluid dynamics equations are discretized in spatial coordinates using integral formulation in conjunction with finite volume method which reduces the governing equations to semi-discretized ordinary differential equations. Temporal integration is performed employing multistage Runge-Kutta time-stepping scheme. A local time step is used to achieve steady-state solution. The numerical computation is carried out on a mono-block with structured grids. The flowfield features over the sharp-tipped double cone configuration such as conical shock wave, separation region, separation and reattachment shock wave and bow shock wave in the cone region, expansion fan, and recirculation flow in the base region are well captured at Mach number 3 and 6 which are identical to the Edney VI type shock interaction. The velocity vector, Mach contours plots and variations of surface pressure coefficient along the sharp-tipped double cone configuration are analyzed at various Mach numbers. The fore-body aerodynamic drag is calculated employing computed pressure distribution. The paper presents the influence of the freestream Mach number on the flows with shock interactions over the sharp-tipped double cone geometry.

***Key words**: CFD, Compressible flow, Gas dynamics, Laminar flow, Shock wave*

Introduction

The hypersonic flow past sharp-tipped double-cone geometry is an interesting case for numerical simulations, because it produces many complex flow field phenomena such as shock wave interactions, triple points, recirculation zones at high speed flow. Interactions of shock waves with laminar boundary layer are in practical applications and have been investigated experimentally and numerically. Laminar shock interaction on the double-cone configuration consists of two-different cone half-angles with an upstream 25 deg section followed by a downstream 55 deg section has been the subject of intense research interest for over two decades. The sharp-tipped double cone axisymmetric configuration is also one of the reentry modules and having an attached oblique shock wave as compared to the detached shock wave of the truncated spherical-cone reentry capsule [1]. Experimental and numerical studies of the laminar separation in hypersonic flow have been carried out by many investigators [2 - 4] to understand the physics of flows over double-cone geometry. The recent experimental investigations [5] on the double-cone model reveal that the size of the separation bubble is significantly affected by an applied magnetic field.

Prabhu et al. [6] and Gaitonde and Shang [7] have computed heat transfer and skin friction coefficient in laminar flow conditions. The flowfield features of shock waves interaction include location of separation, surface pressure variation, and shock structure. It has been also observed that these flow field are controlled by the vorticity in the incoming boundary layer and the strength and the orientation of the shock wave.

Figure 1 shows a schematic of a sharp-tipped double-cone flowfield at high speed. The flowfield emanates the separation shock wave induced by the flow deflection due

Paper Code : V67 N1/850-2015. Manuscript received on 27 Jan 2014. Reviewed, revised and accepted as a Full Length Contributed Paper on 07 Oct 2014

to the flow separation on the ramp section of the cone, and the inner reattachment shock, induced by the final reflection of the flow at the ramp do not cross each other, because they belong to the same family. They meet in the triple point and form a single stronger shock, the outer reattachment shock. A slip line and an expansion fan originate at the triple point. The complex flowfield over the double cone needs numerical simulations in order to know the effects of variations of freestream Mach number.

The main focus of the present paper is to numerically analyze shock wave-boundary layer interaction over a sharp-tipped double cone for freestream Mach number range of 2, 3 and 6. The numerical simulation is to solve axisymmetric laminar compressible time-dependent Navier-Stokes equations employing a multi-stage Runge-Kutta time stepping scheme. The numerical scheme is second-order accurate in space and time. A local time step is employed to obtain a steady-state numerical solution. The computation is carried out on a mono-block with structured grid arrangement. The effects of freestream Mach number over the axisymmetric a sharp-tipped double cone configuration are numerically analyzed employing velocity vector, contour plots and variation of pressure coefficient along the surface of the double cone model. Fore-body aerodynamic drag coefficient is obtained using the computed pressure profile at various Mach number.

Governing Equations

The axisymmetric time-dependent laminar compressible Navier-Stokes equations were written in the integral form, and the system of equations was augmented by the perfect gas law for the numerical simulation. The coefficient of molecular viscosity was calculated using Sutherland's law. The flow is assumed to be laminar, which is consistent to the experimental and numerical of earlier investigators [2 - 4].

Numerical Schemes

Spatial Discretization

The governing fluid dynamics equations are written in the integral formulation in conjunction with finite volume method in order to facilitate the spatial discretization. The flowfield code employs a finite volume discretization technique on a structured non-overlapping quadrilateral mesh. The spatial and temporal terms are decoupled using the method of lines. The flux vector is divided into the inviscid and viscous components [8]. The discretized solution to the governing equations results in a set of volume-averaged state variables of mass, momentum, and energy. A cell centre scheme is used to store the flow variables. The numerical procedure reduces to central differencing on a smooth varying grid in the computational domain. The entire spatial discretization scheme is second order accurate. The cell-centered spatial discretization scheme is non-dissipative; therefore, artificial dissipation terms are added as a blend of a Laplacian and biharmonic operator in a manner analogous to the second and fourth differences. The artificial terms [9] are added explicitly to prevent numerical oscillations near shock waves to damp high frequency unstable modes.

Temporal Discretization

Temporal integration is carried out using three-stage Runge-Kutta time-stepping scheme of Jameson et al. [8]. The artificial dissipation terms are evaluated only at the first stage. The scheme is stable for a Courant number less than or equal 2. Local time steps are used to accelerate convergence to a steady-state numerical solution by setting the time step at each point to the maximum value allowed by the local Courant-Friedrichs-Lewy condition. The present numerical algorithm is validated with many test cases [10, 11].

Initial and Boundary Conditions

The freestream conditions for each trajectory point are enumerated in Table-1 which is used as the initial conditions. M, p and T represent Mach number, pressure and temperature, respectively. The subscript ∞ represents freestream value in the table. All the flow variables are extrapolated at the outer boundary and no-slip condition is used as wall boundary condition. An isothermal wall condition has been considered for the surface of the sharp-tipped double cone model. A symmetry condition is applied on the centre line ahead as well as downstream of the sharp-tipped double cone.

Table-1 : Trajectory Points and Initial Conditions

M_∞	p_∞, Pa	T_∞, K
2.0	2891	219
3.0	2073	224
6.0	1238	232

Geometrical Detail of Sharp-Tipped Double Cone

The geometrical detail of the sharp-tipped double cone configuration is displayed in Fig.2. The double-cone configuration consists of two-different cone half-angles with an upstream 25 deg section followed by a downstream 55 deg section. The model is truncated with a right circular cylinder as seen in the figure. The diameter of the first and second cones is 8.58 cm and 26.16 cm, respectively. The total length of the double cone model is 19.87 cm.

Computational Grids

One of the controlling factors for the numerical simulation is proper generation of the computational grid. In order to initiate the numerical simulation of the flow along the sharp-tipped double cone model, the physical space is discretized into non-uniform quadrilateral mesh on a mono-block. These body-oriented grids are generated using a finite element method [12] in conjunction with homotopy scheme [13]. These stretched grids are generated in an orderly manner. Grid independence tests are carried out, taking into consideration the effect of the computational domain, the stretching factor to control the grid intensity near the wall, and the number of grid points in the axial and normal directions. The grid-stretching factor in the radial direction is varied 1.5 to 5. The present numerical analysis is carried out on 152 x 52 grid points. The grid-stretching factor is selected as 5, and the outer boundary of the computational domain is kept about 4 to 7 times the base diameter of the model. The computational considered the boundary condition as mentioned by Lunev [14]. The bow shock wave intersects its exit section of the double cone model. The boundary condition cannot be imposed on the exit section of the double-cone model, if the normal Mach number is greater than unity. The finer mesh near the wall helps to resolve the viscous effects. The coarse mesh helps in reducing the computer time. The grid size varies depending on Reynolds number based on the maximum diameter of the double cone model. The minimum mesh size in the normal direction of the sharp-tipped double cone is 1.488×10^{-4} m. Fig.3 shows an enlarged view of the computational grid over the 25/55 deg sharp-tipped double cone configuration. Numerical results are validated with various cone angles and compared with the analytical results and found in good agreement [15, 16]. The computational grid is found to give a relative difference of about ±3% in the computation of the fore-body aerodynamic drag coefficient. The convergence criterion is bases on the difference in density value at any grid points between two successive iterations, the absolute difference between densities to be less than or equal to 10^{-5}.

Results and Discussion

The numerical procedure described in the previous section is applied here to compute the flow field over the 25/55 deg sharp-tipped double cone model for Mach number 2, 3 and 6 and the Reynolds number based on the base diameter of the model are 8.578×10^6, 12.868×10^6 and 25.736×10^6 respectively.

Flow Characteristics

Figure 4 displays the pressure and density contour plot over the sharp-tipped double cone module at $M_\infty = 3$. The pressure contour shows very high pressure in the cone-cone junction due to the bow shock wave interaction region. The shock wave reaches down into supersonic portion of the boundary layer as can be observed in the vector plots. The density plot gives flowfield features in the wake region of the module.

Figure 5(a) - (c) depicts the closed view of velocity vector field at M_∞ = 2, 3 and 6. Despite its geometric simplicity, the double cone generates complex flow field with increasing Mach number. It can be seen from the vector plots that all the significant flow field features are captured by present numerical algorithm such as formation of conical shock, bow shock wave, rapid expansion fan on the corner, flow recirculation region with converging free shear layer and formation of the vortex flow in the aft region of the sharp-tipped double cone configuration. A separation bubble is clearly observed on the vector plots. For the sake of clarity in flow field, Fig.5(c) is shown with skipping few grid points in the vicinity of the wall of the sharp-tipped double cone. The basic flow phenomena of laminar separated cone-cone junction flow are shown in Fig.5(c). The complexity of the flow field increases with the increasing freestream Mach number as observed in Fig.5(a) - (c). The wake flow field exhibits free-shear layer, recompression shock wave and re circulation region. The attached leading conical shock wave interacts with a detached bow shock wave that impinges on the second cone surface. This produces very high surface pressures on the second cone. Because of the high pressures at the impingement location, the flow separates near the cone-cone junction and a recirculation zone develops, which in turn alters the shock interaction. We define flow separation length as the axial distance between the separation and reattachment points obtained from the change of velocity vector in the vector plots of Fig.5. The separation and reattachment points are indicated in Fig.5 by symbols *S* and *R*, respectively. The length of the flow

separation shows of the strength of the interaction. The size of the separation zone is very sensitive the freestream Mach number which changes conical shock wave angle, the bow shock wave profile and thus the strength of the shock interaction. Fig.5 also depicts the Mach contour plots over the double cone body at various values of Mach number. The bow shock wave moves close to the body with the increasing of freestream Mach number. The cone-cone junction creates a complex shock-interaction region where a change in the size of the separated region changes the angles of the intersecting shocks which in turn changes the size of the separated region further. It is important to mention here that the flow field is very sensitive to the freestream Mach numbers. The interaction shown in Fig.5(c) is the Edney type VI interaction [17, 18].

Surface Pressure

Figure 6 shows the pressure coefficient variation $\left[C_p = 2\left\{(p/p_\infty) - 1\right\}/\gamma M_\infty^2\right]$ along the surface for M_∞ = 2, 3 and 6, where γ is the ratio of specific heats. The x/D = 0 location is the stagnation point, where x is distance measured from the stagnation point and D is the base diameter of the model. The model of the double cone is inserted in Fig.6 in order to visualize the flow characteristics as observed in the velocity vector and contour plots. The variations of pressure coefficient on the fore-body show the influence of the freestream Mach numbers. The pressure coefficient distributions depict a pronounced increase at the separation and the reattachment shock. The pressure plateau behind the reattachment point is function of the freestream Mach number. The maximum pressure coefficient is occurred in the vicinity of the reattachment shock wave. The pressure gradually decreases after the reattachment shock. The pressure coefficient suddenly drops in the base region and remains constant over the base of the model.

The fore-body aerodynamic drag coefficient is calculated by integrating the pressure distribution over the sharp-tipped double cone axisymmetric configuration excluding the base of the model. For the calculation of the drag coefficient the reference area is taken as the area of the base of the module. The values of the aerodynamic drag coefficients are 1.24, 1.36 and 1.39 for Mach number 2, 3 and 6, respectively.

Conclusions

Flowfield over the sharp-tipped double cone is computed by solving compressible axisymmetric laminar Navier-Stokes equations for freestream Mach numbers range of 2, 3 and 6. The numerical simulation is carried out employing finite volume method. The time step is local on the computational domain. A single block structured computational grid is used in the numerical simulation. The computed flowfield over the double cone model depicts all the essential flow characteristics such as formation of the conical and the bow shock waves, expansion and compression fan, recirculation region. The surface pressure coefficient variations along the double cone reentry configuration are computed for various different freestream Mach numbers. The influence of freestream Mach numbers over the fore body of the double cone is numerically investigated. The flow about a double cone is well suited for this type of study because the shock interaction and the size of the separation zone strongly depend on the global features of the flow. The computational obtained flow field images such as vector and contour plots exhibit all the shock interactions details at high-speed flow over the double cone configuration. The values of the fore-body aerodynamic drag coefficients are calculated by integrating pressure profile over the model.

References

1. Mehta, R. C., "High Speed Field Analysis for Satellite Launch Vehicle and Reentry Capsule", Journal of Magneto-hydrodynamics, Plasma and Space Research, Vol.15, No.1, 2010, pp.53-100.

2. Chanetz, B., Benay, R., Bousquet, J.-M., Bur, R., Oswald, J., Pot, T., Grasso, F and Moss, J., "Experimental and Numerical Study of the Laminar Separation in Hypersonic Flow", Aerospace Science and Technology, Vol.10, No.3, 1998, pp.205-218.

3. MacLean, M., Wadhams, T., Holden, M and Candler, G., "Integration of CFD and Experiments in the Cubrc Lens Shock Tunnel Facilities to Understand the Physics of Hypersonic and Hypervelocity Flows", 4th Symposium on Integrating CFD and Experiments in Aerodynamics von Karman Institute, Rhode-Saint-Gense, Belgium, 14-16 September 2009.

4. Wright, M. J., Sinha, K., Olejniczak, J., Candler, G. V., Magruder, T. D and Smits, A. J., "Numerical and Experimental Investigation of Double-Cone Shock Interactions", AIAA Journal, Vol.38, No.12, December, 2000, pp.2268-2276.

5. Nagata, Y., Yamada, K and Abe, T., "Hypersonic Double-Cone Flow with Applied Magnetic Field", Journal of Spacecraft and Rockets, Vol.50, No.5, 2013, pp.981-991.

6. Prabhu, R., Stewart, J and Theraja, R., "Shock Interaction Studies on a Circular Cylinder at Mach 16", AIAA Paper 90-0606, 1990.

7. Gaitonde, D and Shang, J., "Accuracy of Flux Split Algorithms in High Speed Viscous Flows", AIAA Journal, Vol.31, No.7, 1993, pp.1215-1221.

8. Peyret, R and Vivind, H., Computational Methods for Fluid Flow, Springer-Verlag, 1993, pp.109-111.

9. Jameson, A., Schmidt, W and Turkel, E., "Numerical Solution of Euler Equations by Finite Volume Methods Using Runge-Kutta Time Stepping Schemes", AIAA Paper 81-1259, 1981.

10. Mehta, R. C., "Flow Field Simulation Over Reentry Modules at High Speed", Journal of Aerospace Sciences and Technologies, Vol.62, No.1, February, 2010, pp.55-65.

11. Mehta, R. C., "Numerical Simulation of the Flow Field Over Conical, Disc and Flat Spiked Body at Mach 6", The Aeronautical Journal of the Royal Aeronautical Society, Vol.114, No.1154, 2010, pp.225-236.

12. Mehta, R. C., "Block Structured Finite Element Grid Generation Method", Computational Fluid Dynamics Journal, Vol.18, No.2, 2011.

13. Shang, J. S., "Numerical Simulation of Wing-fuselage Aerodynamic Interaction", AIAA Journal, Vol.22, No.10, 1984, pp.1345-1353.

14. Lunev, V., Real Gas Flows with High Velocities, CRC Press, USA, 2009, pp.247-249.

15. Mehta, R. C., "High Speed Flow over Spiked Blunt Body and Representation of Shock Polar", Computational Fluid Dynamics Journal, Vol.18, No.3, 2009, pp.22-30.

16. Mehta, R. C., "Computations of Flow Field Over Reentry Modules at High Speed", Computational Simulations and Applications, Edited by J. Zho, INTECH Open, Croatia, 2011, pp.347-372.

17. Edney, B., "Anomalous Heat Transfer and Pressure Distributions on Blunt Bodies at Hypersonic Speeds in the Presence of an Impinging Shock", FFA Report 115, 1968.

18. Hirschel, E. H., Basics of Aerothermodynamics, Springer (India) Private Limited, New Delhi, 2008.

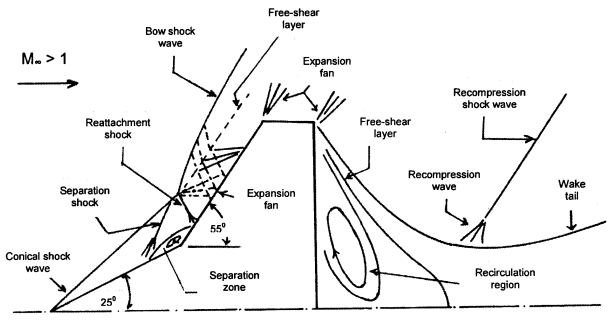

Fig.1 Schematic of the High Speed Flow Past Sharp-tipped Double Cone Geometry

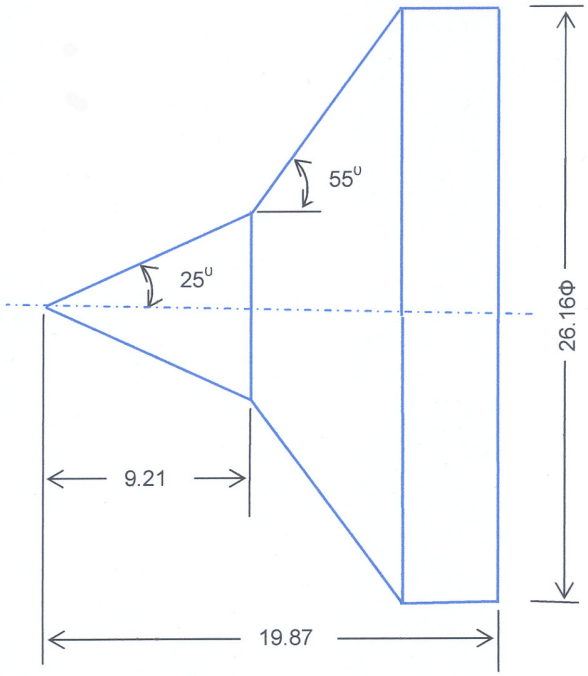

Fig.2 Geometry of the Sharp-tipped Double Cone

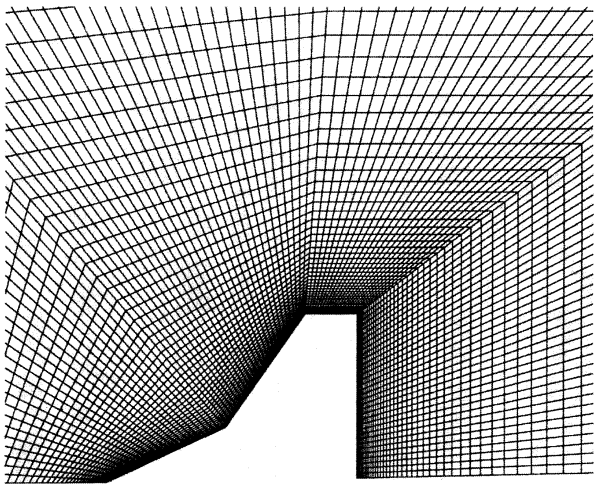

Fig.3 Close-up View of Computational Grid Over a Sharp-tipped Double Cone

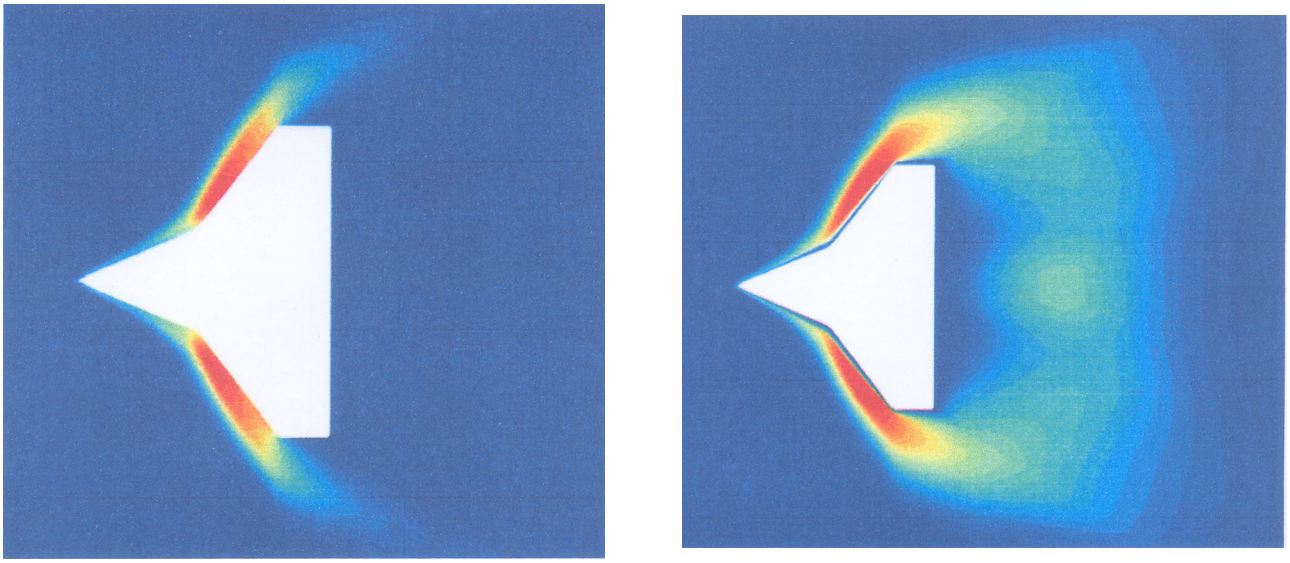

Fig.4 Pressure and Density Contour Plots Over the Sharp-tipped Double Cone, $M_\infty = 3.0$
(a) Pressure Contour Plots (b) Density Contour Plots

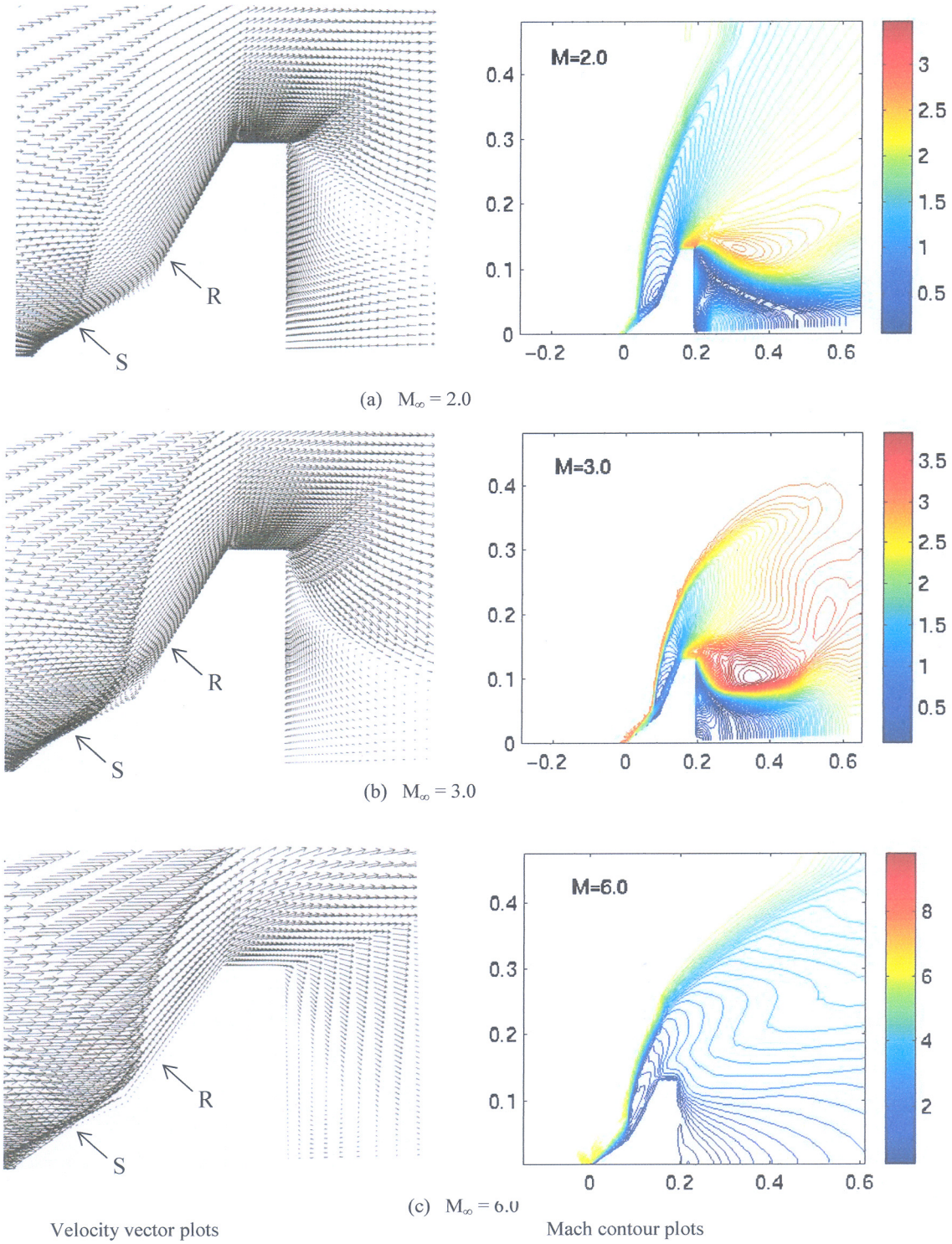

Fig.5 Velocity and Mach Contours Plots Over the Sharp-tipped Double Cone

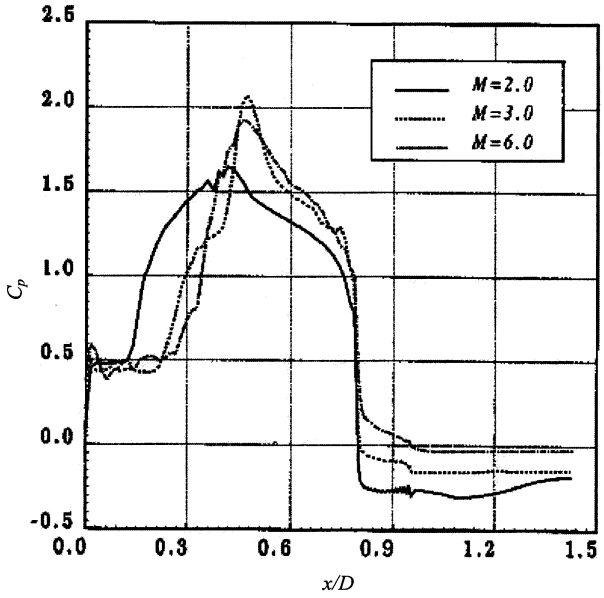

Fig.6 Variation of Pressure Coefficient Along the harp-tipped Double Cone